The effect of antimony in the growth of indium arsenide quantum dots in gallium arsenide (001)

Y. Sun, S. F. Cheng, G. Chen, and R. F. Hicks[a)]
Chemical Engineering Department, University of California, Los Angeles, California 90095

J. G. Cederberg and R. M. Biefeld
Sandia National Laboratories, P.O. Box 5800, Albuquerque, New Mexico 87185-0601

(Received 22 April 2004; accepted 16 December 2004; published online 8 February 2005)

The effect of an initial saturation coverage of antimony on the growth of indium arsenide quantum dots on gallium arsenide has been studied during metalorganic vapor-phase epitaxy. After depositing one to two bilayers of InAs at 723 K, the samples were quenched, transferred to ultrahigh vacuum, and characterized by scanning tunneling microscopy and x-ray photoelectron spectroscopy. It has been found that the critical thickness for onset of quantum dot formation is 33% less with Sb present as compared to without Sb. The antimony incorporates into the quantum dots, increasing their density and total volume, and causing them to be more densely clustered together. © *2005 American Institute of Physics*. [DOI: 10.1063/1.1858054]

I. INTRODUCTION

Nanoscale control of epitaxial growth processes is essential in realizing advanced optical and electronic devices. For example, record high electron mobilities have been attained in compositionally strained, III-V semiconductor heterostructures, where the film thickness is on the order of a few nanometers.[1] At higher levels of lattice mismatch, the heteroepitaxial layers can be made to self-assemble into quantum dots (QDs).[2] These nanostructures have been fabricated into solid-state lasers that exhibit low threshold current densities and a high characteristic temperature T_0.[3,4] In order to exploit the attractive properties of these materials, one must have a detailed understanding of the relationship between the growth process and the QD composition and structure.

Quantum dots form via a Stranski–Krastonov (SK) growth mode, in which a thin wetting layer is produced, followed by the appearance of three-dimensional (3D) islands.[2,5–7] The nucleation and growth of the QDs depends on many factors, including lattice strain, surface and interfacial energy, and growth kinetics. To suppress the formation of large phase-segregated islands, a low substrate temperature and high growth rate are employed.[2] One may further influence QD formation by employing "surfactants," such as antimony, bismuth, and tellurium, which presumably aid two-dimensional growth and increase the critical thickness for the 2D to 3D transition.[8–10] In some cases, surfactants have been found to narrow the size distribution and increase the density of QDs.[8,10]

Several research groups have investigated the use of antimony as a surfactant during the growth of III-V compound semiconductors. Yang *et al.*[11,12] found that it enhanced the 2D morphology of strained InGaAsN quantum wells on GaAs, thereby improving the optical properties of the laser structure. Stringfellow and co-workers[13] reported that Sb addition during InGaP epitaxy on GaAs decreases the order parameter of the alloy by relieving the surface strain energy during growth. Incorporation of small amounts of antimony during the self-assembly of InAs quantum dots on GaAs may provide beneficial surfactant effects. On the other hand, since Sb has a small miscibility gap with InAs, it might not segregate to the growth front as efficiently, and instead may substitute for some of the As in the group V sublattice. Nevertheless, this alloy may be of interest, since QDs made from this material would exhibit a smaller band gap, suitable for long wavelength devices (>1.3 μm).

In this work, we have investigated the metalorganic vapor-phase epitaxy of InAs quantum dots on GaAs (001) with and without the predeposition of antimony. Scanning tunneling microscopy (STM) and x-ray photoelectron spectroscopy (XPS) were used to characterize the nanostructures immediately following deposition. We have found that in the presence of Sb, the amount of InAs needed for quantum dot formation decreases substantially and that the Sb incorporates into the quantum dots.

II. EXPERIMENTAL METHODS

The epitaxial materials were deposited in a Veeco (formerly Emcore) Discovery-125 MOVPE system. The reactor was maintained at 60 Torr with a flow of 37.0 standard l/min of ultrahigh-purity hydrogen. The H_2 was passed through a SAES Pure Gas, Inc. purifier (model PS4-MT3-H) that removed any remaining oxygen, nitrogen, or carbon species to below a few parts per billion. The GaAs (001) substrates were Si doped to 1.0×10^{18} cm^{-3} and were 0.5° miscut towards [−110] direction. A gallium arsenide buffer layer, 0.25 μm thick, was grown using tertiarybutylarsine (TBAs) and trimethylgallium (TMGa) at 590 °C. Then the samples were cooled to 450 °C at 0.72 °C/s in TBAs and hydrogen. On some of the samples, antimony was dosed onto the GaAs surface by feeding 6.0×10^{-5} mol/min trimethylantimony (TMSb) for 90 s. A 5 s interruption with hydrogen flow was

[a)]Author to whom correspondence should be addressed; electronic mail: rhicks@ucla.edu

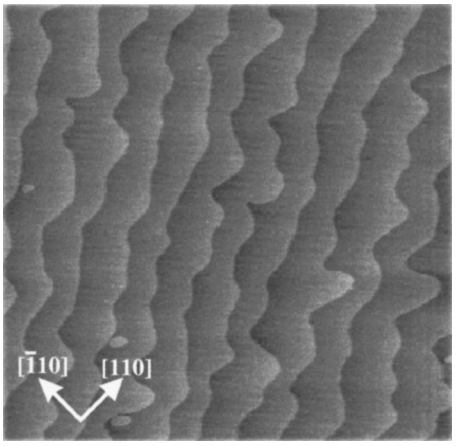

FIG. 1. Scanning tunneling micrograph of the GaAs (001) surface (image size 2×2 μm^2; current=1 nA; and bias=−3 V).

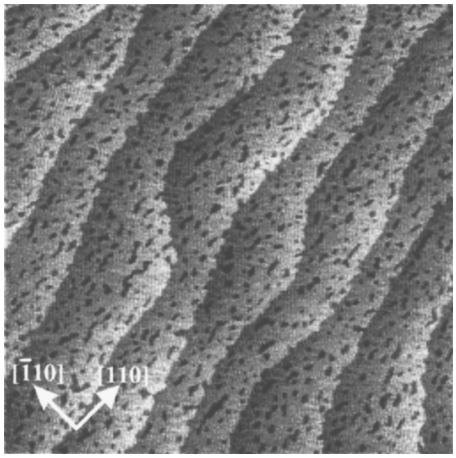

FIG. 2. Scanning tunneling micrograph after MOVPE of InAs on GaAs for 14 s (image size 1×1 μm^2; current=0.5 nA; and bias=−2 V).

employed before InAs deposition to purge the residual TMSb out of the reactor. Next, InAs was deposited by feeding TBAs and trimethylindium (TMIn) at 4.6×10^{-4} and 7.3×10^{-6} mol/min, respectively, for 10–20 s. These process conditions yield a growth rate of 0.30 ± 0.05 Å/s for lattice matched films. Finally, the samples were quenched in H_2 at 1.0 °C/s and transferred to an ultrahigh vacuum (UHV) chamber without exposure to air.

The films were analyzed by XPS and STM in the UHV system. Core level photoemission spectra of Ga $2p_{3/2}$, In $3d_{5/2}$, As $3d$, As $2p_{3/2}$, Sb $3d_{5/2}$, and Sb $2p_{3/2}$ lines were collected with a Physical Electronics intrument 3057 XPS spectrometer, using aluminum K_α x rays ($h\nu$ =1486.6 eV). All XPS spectra were taken in small area mode with a 7° acceptance angle and 23.5 eV pass energy. The detection angle with respect to the surface normal was 25°. The STM micrographs were obtained using a Park Autoprobe/VP scanning tunneling microscope. Tunneling was out of filled states with a sample bias of −2.0–−4.0 V and a tunneling current of 0.5–1.0 nA. Statistical analysis of the STM line scans (15 samples), using different image sizes, scanning rates, and tunneling currents, revealed that the lateral and vertical dimensions of a feature were reproduced to within ±4% and ±10%, respectively.

III. RESULTS

A. The growth of InAs quantum dots without Sb

Shown in Fig. 1 is an STM micrograph of the GaAs (001) surface after depositing a 0.25 μm thick buffer layer and transferring the sample from the MOVPE reactor to the UHV system. The surface contains atomically flat terraces with an average width of 0.14 μm. This terrace width corresponds to a substrate miscut of ~0.1°. Examination of the surface by low-energy electron diffraction indicates that it exhibits a $c(4\times4)$ reconstruction with an As coverage of ~1.75 ML (ML—monolayer).[14]

Shown in Fig. 2 is an STM micrograph of a sample following MOVPE of InAs on GaAs for 14 s. This run time should deposit ≈4.2 Å of InAs, which corresponds to 1.4 bilayers (BL). The morphology of the surface remains flat, but with many pits on the terraces, one bilayer deep, and with indentations along the step edges. X-ray photoelectron spectra indicate that it contains 10.8 at. % indium. Thus, a thin InAs wetting layer has been deposited, which is below the critical thickness θ_{crit} for quantum dot formation.[15] The atomic concentration of the other elements detected by XPS is summarized in Table I.

The overlayer thickness indicated above is obtained from growth rate measurements on bulk, lattice-matched films. In order to check this value for growth of very thin layers, a model is presented to estimate the overlayer thickness from the XPS data. The intensity of the photoelectrons generated by x-ray bombardment follows an exponential decay function with a characteristic escape length:[16,17]

TABLE I. The surface atomic percentage and estimated overlayer thickness.[a]

Sample	Ga atom% (Ga $2p_{3/2}$)	In atom% (In $3d_{5/2}$)	As atom% (As $2p_{3/2}$)	Sb atom% (Sb $3d_{5/2}$)	Deposition time (s)	Overlayer thickness (BL)
Figure 1	35.1	···	64.9	···	···	···
Figure 2	23.1	10.8	66.1	···	14.0	1.4
Figure 3	20.4	13.8	65.8	···	18.0	1.8
Figure 5	20.8	13.1	66.1	···	12.0	1.8
Sb:GaAs	35.8	···	58.5	5.7	···	···
Figure 7	26.5	9.5	58.1	5.9	10.0	1.0
Figure 8	25.2	11.0	58.3	5.5	14.0	1.4
Figure 10	24.5	11.4	58.5	5.6	18.0	1.8

[a]Atomic percentages are calculated excluding carbon.

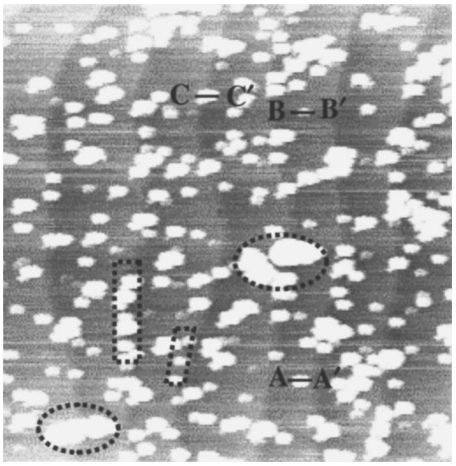

FIG. 3. Scanning tunneling micrograph after MOVPE of InAs on GaAs for 18 s (image size 0.8×0.8 μm^2; current=0.5 nA; and bias=−2 V).

$$I_S = I_S^{\infty} \exp\left(-\frac{d_{ov}}{\lambda_{ov}\cos(\alpha)}\right), \tag{1}$$

where I_S and I_S^{∞} are the integrated peak intensities with and without the overlayer, λ_{ov} is the photoelectron mean free path, equal to 10.3 Å,[18] and α is the detection angle with respect to the surface normal. The overlayer thickness d_{ov} is obtained by solving Eq. (1) explicitly for this variable. Since both the substrate and the film contain arsenic atoms, it is convenient to use the Ga $2p_{3/2}$ peak intensities in Eq. (1) to obtain the InAs thickness. Note that the coverage in terms of bilayers (1 BL=3.0 Å) can be calculated as $d_{ov}/3.0$. It is estimated that for the sample presented in Fig. 2, 4.0 ± 0.4 Å of InAs were deposited, corresponding to 1.3 ± 0.1 BL. This value is the same within the experimental error of the thickness obtained by multiplying the MOVPE run time by the bulk growth rate. The uncertainty in the InAs bilayer value of ±0.1 BL was obtained by reproducing the experiment for three samples. Our experience is that the Veeco D 125 reactor is able to reproducibly grow thin films at ±0.05 Å/s over many runs, and that the growth time should serve as an accurate measure of the amount of InAs deposited in this study. The deposition time and overlayer thickness for all films examined in this work are summarized in the last two columns of Table I.

Shown in Fig. 3 is an STM picture of InAs quantum dots deposited on the GaAs (001) surface at 450 °C for 18 s, yielding an equivalent thickness of 1.8 BL. An atomically flat layer underneath the QDs can still be discerned in the image. An average of 40%±10% of the nanoscale features are aligned along the step edges as shown in the dashed boxes. In addition, dots of different lengths and heights coexist. Line scans across positions *AA′*, *BB′*, and *CC′* in Fig. 3 are presented in Fig. 4. The size of the large quantum dot is 65 nm wide by 5.0 nm high and that of the small one is 30 nm wide by 2.6 nm high. Some of the quantum dots result from coalescence of two dots as shown in Fig. 4, *CC′*, where the line scan contains two peaks. Clusters are also observed, for example, in the circles highlighted in Fig. 3. The QD

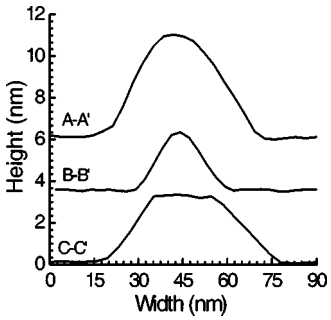

FIG. 4. Line scans of the STM image in Fig. 3 across *AA′*, *BB′*, and *CC′*.

density is estimated to be 3.5×10^{10} cm^{-2} by averaging three locations on each of three samples grown under the same conditions.

We grew two additional samples with the same amount of InAs as those in Figs. 2 and 3. The only difference is that the TMIn flow, and in turn the growth rate, was increased 50%, and the growth time shortened accordingly. For the 1.3 BL sample, the morphology observed in the STM micrograph is identical to that in Fig. 2. The initial stage of InAs growth is the formation of a two-dimensional, pitted wetting layer. With further deposition of InAs, QDs are again observed as demonstrated in Fig. 5. In contrast to Fig. 3, these quantum dots are smaller and the size distribution is narrower. Figure 6 shows the line scans across *DD′* and *EE′* from Fig. 5. The size of the large dot is 25 nm wide by 1.3 nm high, while that of the small one is 15 nm wide by less than 1.0 nm high. For this sample, the density of the dots is estimated to be 9.0×10^{10} cm^{-2} (three locations on two samples).

B. The growth of InAs with predeposition of Sb

Before InAs deposition at 450 °C, the GaAs (001) surfaces were exposed to a Sb flux of 6.0×10^{-5} mol/min for 90 s. To make sure the starting surface was flat, growth was interrupted, and the sample characterized by STM in the UHV system. It was found that the surface is covered with smooth terraces similar to the GaAs buffer layer. This indi-

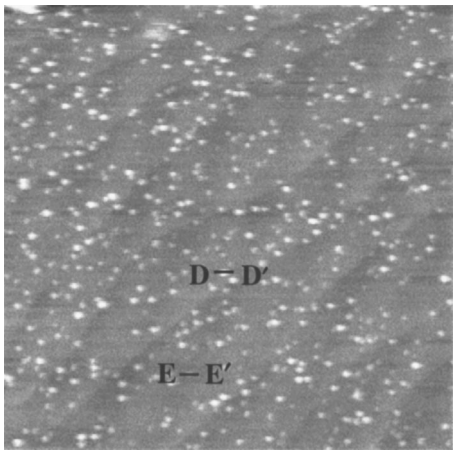

FIG. 5. Scanning tunneling micrograph after MOVPE of InAs on GaAs for 12 s with a 50% increase in TMIn feed rate (image size 0.8×0.8 μm^2; current=0.5 nA; and bias=−2 V).

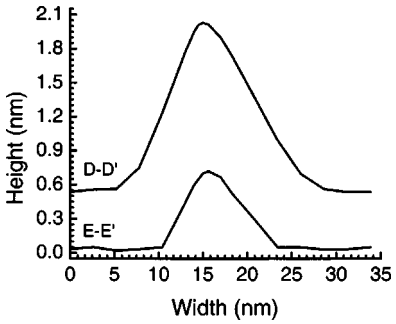

FIG. 6. Line scans of the STM image in Fig. 5 across DD' and EE'.

cates that Sb does not diffuse into the bulk and create a strained GaAsSb film, which would disrupt the terrace structure.[19] The XPS data show that the surface contains 5.7% Sb, 58.5% As, and 35.8% Ga (cf., Table I). Compared to the XPS data for the pure GaAs film, it appears that antimony atoms replace some of the arsenic atoms on the surface.[20] We also exposed the sample to the TMSb flow for 60 s and recorded the same XPS and STM data. This suggests that a 90 s exposure of TMSb at 450 °C is sufficient to saturate the GaAs (001) surface. The Sb coverage is estimated to be 0.85 ± 0.05 ML using a XPS model developed earlier,[21,22] and is consistent with the composition obtained by Whitman and coworkers in their thorough study of this surface.[20]

Shown in Fig. 7 is an STM micrograph of the sample following MOVPE of InAs on Sb:GaAs at 450 °C for 10 s. The amount of InAs deposited in this case is ~1.0 BL. The image shows that the surface is covered with many small terraces one bilayer high. A few 3D islands are present and are circled in the figure. These small dots are 6.0 Å high and their density is low ($\sim 3 \times 10^8$ cm^{-2}). It is surprising to see these dots at such a low InAs coverage. We showed earlier that without Sb predeposition, up to 1.4 BL of InAs can be deposited before the 3D features start to appear.

Presented in Fig. 8 is an STM image of the sample following MOVPE of InAs on Sb:GaAs for 14 s. This growth time corresponds to 1.4 BL of InAs. A dramatic change in the morphology is observed with the appearance of densely packed 3D features. The surface contains agglomerated islands as well as single quantum dots. On the graph, the height difference between the darkest and the brightest feature is 6.0 nm. Shown in the inset is a 0.50×0.25 μm^2 image of the same area. Its contrast is adjusted so that the underlayer is resolved. Atomic steps are clearly seen and the terraces have pits in them one bilayer deep.

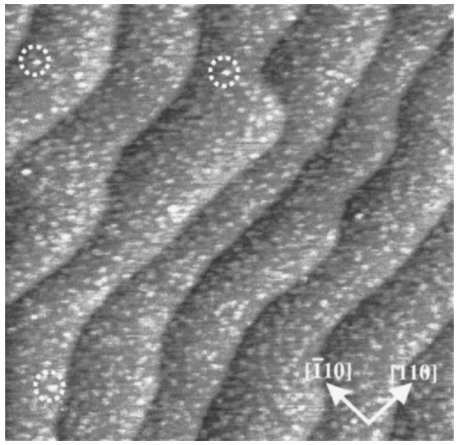

FIG. 7. Scanning tunneling micrograph after MOVPE of InAs on Sb:GaAs for 10 s (image size 1×1 μm^2; current=0.5 nA; and bias=−2 V).

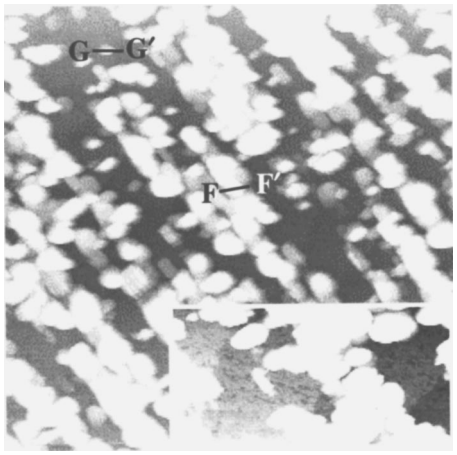

FIG. 8. Scanning tunneling micrograph after MOVPE of InAs on Sb:GaAs for 14 s (large image size: 1×1 μm^2; small image size 0.50×0.25 μm^2; current=0.5 nA; and bias=−2 V).

Two line scans were taken of the features in Fig. 8, across FF' and GG'. These scans are presented in Fig. 9. In the former case, a peak with two shoulders is recorded, indicating that a smaller 3D feature has nucleated and grown on top of a larger one. The line scan through GG' reveals a single quantum dot that is 47 nm wide by 2.7 nm high. The density of the 3D islands is $\sim 6.0 \times 10^{10}$ cm^{-2}.

When 1.8 BL of InAs is deposited, the surface is covered with mounds and clusters. Figure 10 shows a 1.0×1.0 μm^2 STM micrograph of this nanostructure. On the graph, the height difference between the darkest and the brightest feature is 6.0 nm. One sees that clusters have nucleated and grown on top of the mounds, producing a continuous 3D film. It should be noted that the overlayer evolves into a rough film when less than 2.0 BL of InAs is deposited.

The binding energies of the elements on the semiconductor surfaces are summarized in Table II. For all the samples studied, the gallium and arsenic $2p_{3/2}$ peak positions are constant to within ±0.05 eV. On the other hand, the In $3d_{5/2}$ line shifts 0.31 eV lower in energy when antimony is added to the GaAs surface. Similarly, the Sb $3d$ binding energy decreases

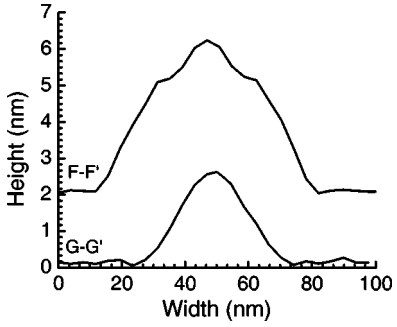

FIG. 9. Line scans of the STM image in Fig. 8 across FF' and GG'.

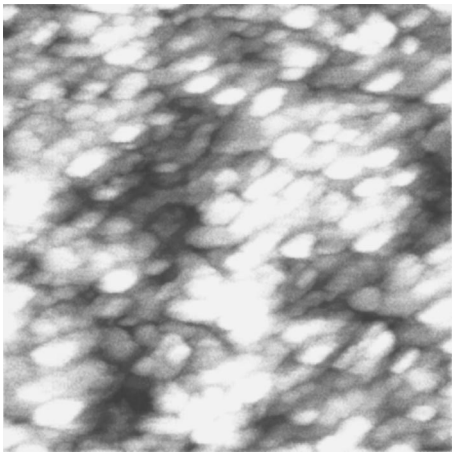

FIG. 10. Scanning tunneling micrograph after MOVPE of InAs on Sb:GaAs(001) for 18 s (image size 1×1 μm^2; current=0.5 nA; and bias $=-2$ V).

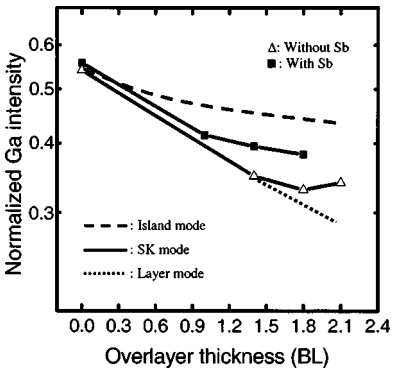

FIG. 11. The dependence of the normalized Ga $2p$ photoemission intensity on the amount of InAs deposited on the GaAs (001) surface.

0.16 eV upon the deposition of indium arsenide. These results indicate that there is a significant chemical interaction between the antimony and the InAs quantum dots.

Finally, shown in Fig. 11 is the effect of the amount of InAs deposited on the integrated intensity of the substrate Ga $2p_{3/2}$ photoemission peak. The trend observed in this plot depends upon the growth mode exhibited by the film, whether it is layer by layer, three dimensional, or layer by layer followed by three dimensional.[23] For the latter Stranski–Krastonov mode, the peak intensity will initially follow an exponential decay, but then shift to a gradual decrease with further deposition time. The change in slope occurs at the transition between the 2D and 3D growth mechanisms. As can be seen in the figure, the indium arsenide films exhibit SK behavior. Transition points of 1.0 and 1.5 BL are obtained for InAs deposition with and without Sb, respectively. The dashed and dotted lines in the figure illustrate the trends expected for the island and layer-by-layer growth modes.[23]

IV. DISCUSSION

Addition of antimony to the gallium arsenide surface has a strong effect on the nucleation and growth of indium arsenide quantum dots. We see that nucleation occurs with $\approx$50% less InAs when Sb is present on the surface. In addition, the density of the QDs is $\sim6.0\times10^{10}$ cm^{-2} on Sb:GaAs versus 3.5×10^{10} cm^{-2} on GaAs alone. Comparison of Fig. 8 to Fig. 3 reveals that the antimony causes the quantum dots to be more tightly clustered together, leading to coalescence and the growth of small 3D structures on top of larger ones.

TABLE II. Binding energies of the elements on the sample surfaces.

Sample	Ga $2p_{3/2}$ (eV)	In $3d_{5/2}$ (eV)	As $2p_{3/2}$ (eV)	Sb $3d_{5/2}$ (eV)
GaAs	1117.02 (0.05)	···	1322.74 (0.04)	···
InAs QD	1117.04 (0.04)	442.09 (0.04)	1322.74 (0.05)	···
Sb:GaAs	1116.99 (0.05)	···	1322.75 (0.03)	526.57 (0.05)
InAs on Sb:GaAs	1117.01 (0.04)	441.78 (0.05)	1322.73 (0.06)	526.41 (0.05)

Relative to the C 1*s* peak at 284.00 eV. Numbers in parenthesis are standard deviations.

We have estimated the quantum dot volume in Fig. 8 using STM line scans and assuming a half-ellipsoid shape for the islands.[24] The height and lateral dimensions for each individual island was measured over a 1.0×1.0 μm^2 area. A surprisingly high value of 2.1 ± 0.4 BL is obtained from this estimate. The 1.4 BL InAs deposited cannot account for this amount of material. Assuming the STM volume estimate is correct, a reasonable explanation would be that the 0.85 ML of antimony incorporates into the quantum dots, presumably bringing with it an equal amount of gallium. Adding 0.85 BL of GaSb to 1.4 BL InAs yields 2.25 BL of total QD volume, in agreement with the line scans.

Further evidence for the incorporation of some substrate material into the quantum dots is obtained from the STM images. Prior to dot nucleation, the InAs overlayer on the Sb:GaAs surface consists of a dense array of small terraces 1.0 BL high, as shown in Fig. 7. After the QDs form, the substrate surface exposed in between the dots is covered with pits 1.0 BL deep. These pits can be seen in the inset picture in Fig. 8. The transformation of the substrate surface from a terraced to a pitted structure suggests that some gallium may incorporate into the indium arsenide quantum dots. The rough, 3D morphology seen in Fig. 10 also suggests that Ga may migrate into the overlayer, since the volume of these structures cannot be accounted for solely by the deposition of 1.8 BL of InAs.

Gallium out-diffusion has been observed previously for GaAs MOVPE. Begarney *et al.*[25] found that upon decreasing the V/III ratio during growth, a pitted layer is produced at intermediate arsenic coverages between the $c(4\times4)$ and (2×4) reconstructions. The (2×4) phase with $\theta_{As}=0.75$ ML initially nucleates on top of the $c(4\times4)$ domains with $\theta_{As}=1.75$ ML. The gallium required for nucleation of the new phase must come from the underlying layer. This results in the formation of pits, 1.0 BL deep, on the GaAs (001) surface.[25]

The x-ray photoemission results provide evidence for the incorporation of Sb into the InAs quantum dots. The In $3d_{5/2}$ binding energy decreases 0.3 eV when Sb is present on the surface. Likewise, the Sd $3d_{5/2}$ binding energy falls by almost 0.2 eV when InAs is deposited onto the Sb:GaAs(001)

crystal. A negative chemical shift is indicative of a decrease in the oxidation state of the element, due to a reduction in the ionic character of the bonds.[17] This effect can be quantified using the Pauling electronegativity scale.[26] The electronegativity values for the In, As, Sb, and Ga atoms are 1.7, 2.0, 1.9, and 1.6, respectively. The electronegativity differences between In–As, Ga–Sb, and In–Sb are 0.3, 0.3, and 0.2, respectively. Bonds formed between indium and antimony will be less ionic, consistent with the observed shifts to lower binding energy.

The trends in the XPS atomic percentages with Sb and InAs deposition are in line with the views presented above. Referring to Table I, we see that after InAs deposition, the amount of gallium detected on the surface is higher, while the amount of indium detected is lower, if antimony is present. These data support the observation that Sb causes greater consumption of the wetting layer by the quantum dots. On the other hand, deposition of the InAs 3D structures (cf., Figs. 8 and 10) does not significantly change the surface atomic percentage of antimony. Evidently, the Sb is not buried sufficiently within the InAs to cause a significant attenuation of the XPS signal. However, due to the three-dimensional nature of this surface, the distribution of the antimony inside the quantum dots cannot be assessed with these data.

In the MOVPE environment, compound semiconductor surfaces are terminated with the group V elements. These elements form dimer bonds to reduce the number of dangling bonds from two to one. On GaAs, the As–As bonds are under tensile stress, since their distance is 2.50 Å compared to a bulk spacing of 4.0 Å along the [−110] direction.[27] Substitution of Sb for As on the surface will relieve some of this stress due to the longer Sb–Sb bond length of 2.86 Å.[28] The strain between the As–As bonds is even larger on InAs than that on GaAs. Consequently, migration of Sb on top of the InAs will yield a lower overall surface energy and potentially promote the two-dimensional growth of an InAs film. However, the results observed here do not support this scenario. In contrast, our experimental observations suggest that antimony atoms incorporate into the InAs quantum dots and induce extra strain. Incorporation of gallium along with Sb into the quantum dots would compensate part of this added strain. The lattice mismatch between the overlayer and the substrate is smaller for a structure containing InGaAsSb compared to that containing only InAsSb.

V. CONCLUSIONS

When antimony is initially present on the GaAs (001) surface, 1/3 less indium arsenide is needed in order to nucleate and grow the quantum dots. The Sb and possibly the same amount of Ga incorporate into the InAs QDs, increasing their density and size.

ACKNOWLEDGMENTS

This research was supported in part by Northrop Grumman, Epichem, Emcore, and the University of California Discovery program, and in part by the Center for Integrated Nanotechnologies, a U.S. Department of Energy, Office of Basic Energy Sciences nanoscale science research center operated jointly by Los Alamos and Sandia National Laboratories. Sandia National Laboratories is a multiprogram laboratory operated by Sandia Corporation, a Lockheed–Martin Company, for the U. S. Department of Energy under Contract No. DE-AC04-94AL85000. One of the authors, Y. S. would like to thank Professor Lian Li, University of Wisconsin, for his invaluable help with the STM.

[1] K. Ismail, M. Arafa, K. L. Saenger, J. O. Chu, and B. S. Meyerson, Appl. Phys. Lett. **66**, 1077 (1995).
[2] D. Bimberg, M. Grundmann, and N. N. Ledentsov, *Quantum Dot Heterostructures*, 1st ed. (Wiley, Chichester, 1999).
[3] F. Y. Chang, J. D. Lee, and H. H. Lin, Electron. Lett. **40**, 179 (2004).
[4] Y. Qiu, D. Uhl, and S. Keo, Appl. Phys. Lett. **84**, 263 (2004).
[5] L. Samuelson *et al.*, Jpn. J. Appl. Phys., Part 1 **34**, 4392 (1995).
[6] B. R. Bennett, R. Magno, and B. V. Shanabrook, Appl. Phys. Lett. **68**, 505 (1996).
[7] F. Hatami *et al.*, Appl. Phys. Lett. **67**, 656 (1995).
[8] C. S. Peng, Q. Huang, W. Q. Cheng, J. M. Zhou, Y. H. Zhang, T. T. Shengd, and C. H. Tung, Appl. Phys. Lett. **72**, 2541 (1998).
[9] J. Massies, N. Grandjean, and V. H. Etgens, Appl. Phys. Lett. **61**, 99 (1992).
[10] B. N. Zvonkov, I. A. Karpovich, N. V. Baidus, D. O. Filatov, S. V. Morozov, and Y. Y. Gushina, Nanotechnology **11**, 221 (2000).
[11] X. Yang, M. J. Jurkovic, J. B. Herox, and W. I. Wang, Appl. Phys. Lett. **75**, 178 (1999).
[12] X. Yang, J. B. Herox, M. J. Jurkovic, and W. I. Wang, Appl. Phys. Lett. **76**, 795 (2000).
[13] J. K. Shurtleff, R. T. Lee, C. M. Fetzer, and G. B. Stringfellow, Appl. Phys. Lett. **75**, 1914 (1999).
[14] B.-K. Han, L. Li, Q. Fu, and R. F. Hicks, Appl. Phys. Lett. **72**, 3347 (1998).
[15] T. J. Krzyzewski, P. B. Joyce, G. R. Bell, and T. S. Jones, Phys. Rev. B **66**, 121307(R) (2002).
[16] Y. Feurprier, C. Cardinaud, and G. Turban, J. Vac. Sci. Technol. B **16**, 1823 (1998).
[17] L. C. Feldman and J. W. Mayer, *Fundamentals of Surface and Thin Film Analysis* (Elsevier, New York, 1986).
[18] P. J. Cumpson and M. P. Seah, Surf. Interface Anal. **25**, 430 (1997).
[19] D. C. Law, Y. Sun, C. H. Li, S. B. Visbeck, G. Chen, and R. F. Hicks, Phys. Rev. B **66**, 045314 (2002).
[20] L. J. Whitman, B. R. Bennett, E. M. Kneedler, B. T. Jonker, and B. V. Shanabrook, Surf. Sci. **436**, L707 (1999).
[21] D. C. Law, Y. Sun, and R. F. Hicks, J. Appl. Phys. **94**, 6175 (2003).
[22] C. H. Li, Y. Sun, D. C. Law, S. B. Visbeck, and R. F. Hicks, Phys. Rev. B **68**, 085320 (2003).
[23] D. L. Smith, *Thin-film Deposition: Principles and Practice* (McGraw-Hill, New York, 1995).
[24] D. Leonard, K. Pond, and P. M. Petroff, Phys. Rev. B **50**, 11687 (1994).
[25] M. J. Begarney, L. Li, C. H. Li, D. C. Law, Q. Fu, and R. F. Hicks, Phys. Rev. B **62**, 8092 (2000).
[26] L. Pauling, *The Nature of the Chemical Bond*, 3rd ed. (Cornell University, Ithaca, 1960).
[27] W. G. Schmidt and F. Bechstedt, Phys. Rev. B **54**, 16742 (1996).
[28] W. G. Schmidt, Appl. Phys. A: Mater. Sci. Process. **A65**, 581 (1997).